INORGANIC CHEMISTRY FRONTIERS

RESEARCH ARTICLE

View Article Online
View Journal | View Issue

Cite this: *Inorg. Chem. Front.*, 2025, **12**, 1225

Precise control of photoemission and circularly polarized emission achieved through resonant coupling of chiral nanoparticles with Ag particles†

Rongze Ma,[a] Dedan Mu,[a] Yanni Lang,[a] Liang Xu,[a] Haoxin Wang,[b] Songtao Li,[b] Yongjin Li,[a] Zhiguo Song,[a] Dacheng Zhou,[a] Yong Yang,[a] Yugeng Wen,[a] Jin Han *[a] and Jianbei Qiu *[a]

Received 15th October 2024,
Accepted 23rd December 2024

DOI: 10.1039/d4qi02598a

rsc.li/frontiers-inorganic

Chiral materials that possess circularly polarized luminescence (CPL) functionality along with up- and down-conversion luminescence properties present promising research opportunities. However, achieving materials that simultaneously exhibit high luminescence emission efficiency across the visible to near-infrared range while also demonstrating CPL activity remains a significant challenge. Here, we achieve a significant enhancement of luminescence from the visible to near-infrared range as well as modulation of upconversion circularly polarized luminescence (Up-CPL) through the resonant coupling of silver nanoparticles with chiral nanoparticles. Our results show that silver nanoparticles excited by 980 nm light generate localized surface plasmon resonance (LSPR), creating a concentrated electromagnetic field at their surface. The electromagnetic field interacts with the chiral material, amplifying the strength of the chiral field, hereby enhancing the intensity of luminescence from the visible to near-infrared. This study presents a novel approach for enhancing visible to near-infrared luminescence intensity and realizing circularly polarized luminescence by using rare-earth-doped chiral inorganic materials coupled with Ag nanoparticles.

Introduction

Chirality is a fundamental concept in science that plays a crucial role in both luminescence and catalysis.[1] The origins of chirality involve mechanisms of chiral formation in a wide variety of materials.[2] In semiconductors, the origin of chirality is typically related to their crystal structure. For instance, in some semiconductor nanoparticles, chiral morphology can be induced by controlling the growth conditions.[3] In metals, chirality can be triggered by surface effects and crystal defects, which alter the arrangement of atoms on the metal surface, leading to the formation of chiral structures.[4] It has been demonstrated that chiral templates can direct or control the arrangement and assembly of other molecules, clusters, or nanomaterials. This process induces chiral properties in otherwise achiral materials, thereby enabling the achievement of specific chiral functions or characteristics.[5–7] This strategy has been employed in the design of chiral precious metal nanoparticles (NPs) as well as inorganic nanoparticles. Nevertheless, the interaction between chiral molecules and light matter is exceedingly weak. Conversely, artificial chiral structures can produce the near-field effect of 'superchiral' protons, which significantly enhances the interaction between chiral molecules and light.[8] Additionally, plasma-based organic–inorganic co-assembled composites can also provide chiral transfer from non-chiral inorganic upconversion nanoparticles (UCNPs) to chiral plasma nanostructures.[9–11] Currently, studies on chiral plasmonic nanostructures have primarily focused on the effects of size and morphology on the optical properties of single-component systems. However, examining only the optical properties of a single material may overlook the interactions and synergistic effects present in multi-component systems. These interactions can give rise to enhanced optical properties. Consequently, an increasing number of researchers are investigating the potential of combining these nanostructured materials with other substances to enhance their luminescent properties.[12–15]

Chiral plasmonic hybrid nanostructures, an emerging class of chiral families, incorporate multiple engineerable compositions in an individual system, enabling novel chiral light–

[a]*Faculty of Materials Science and Engineering, Key Laboratory of Advanced Materials of Yunnan Province, Kunming University of Science and Technology, Kunming 650093, P. R. China. E-mail: jaakaa@163.com, qiu@kust.edu.cn*
[b]*Department of Mathematics and Physics, North China Electric Power University, 071003 Baoding, China. E-mail: songtaoli2001@126.com*

† Electronic supplementary information (ESI) available. See DOI: https://doi.org/10.1039/d4qi02598a

matter interactions.[16,17] Recent advances have also been made in enhancing chiral signals and extending the response range in the UV, visible and NIR regions due to the optical coupling between different components in the heterostructure of chiral plasmas.[18–20] In addition to these properties and functionalities, composite nanomaterials based on chiral plasma have higher luminescence efficiency compared to single-component NPs. Recently, due to the low upconversion luminescence efficiency, significant research efforts have been dedicated to enhancing the luminescence efficiency of UCNPs.[21–23] In recent years, Liu *et al.* have achieved ultra-bright upconversion luminescence using a nanoparticle emitter-coupled gap plasma mode.[24] Xu *et al.* made significant advances by creating a tilted plasma nanocavity that couples with UCNPs.[25] This innovation greatly reduced the confinement of the 4f–4f forbidden transitions of rare earth ions, leading to a substantial increase in luminescence intensity and a reduction in decay time. Enhanced emission from low quantum yield upconversion nanoparticles through high electric field localization represents a promising application. Although numerous experiments have explored enhancing upconversion luminescence using surface plasmon resonance (SPR) generated by specially designed noble metal nanostructures (*e.g.*, Au, Ag), the intrinsic electronic configuration of these metals often results in a weak SPR response in the ultraviolet (UV) region.[26–28] Consequently, significant plasmonic enhancement is typically observed only in green and red upconversion emissions, with enhancements in the near-infrared (NIR) region being rarely reported.

In this study, we employed Ag particles coupled with chiral inorganic nanoparticles to achieve strong Up-CPL. The prepared nanoparticles demonstrated a marked enhancement in luminescence across both the visible and near-infrared regions, showcasing a narrow and sharp emission specifically in the near-infrared range. In addition, finite-difference time-domain (FDTD) simulations revealed that Ag particles excited by 980 nm light generate LSPR, leading to a highly concentrated electromagnetic field on the particle surface. This field interacts with the chiral material, amplifying the chiral field's strength and significantly improving luminescence from the visible to the near-infrared region. Due to the reduced optical loss of the Ag particles in the near-infrared, Mie scattering produces a stronger resonance effect, which in turn produces a narrow and sharp near-infrared luminescence through the Mie enhancement effect. Composites of noble metal Ag particles combined with chiral inorganic nanoparticles can effectively modulate the emission intensity and polarization of NPs, opening new avenues for applications in imaging, sensing, and anti-counterfeiting.

Experimental section

Materials

The following materials were utilized in the synthesis: erbium oxide (Er_2O_3), D-sorbitol (D-Sor), ytterbium oxide (Yb_2O_3), bismuth nitrate pentahydrate ($Bi(NO_3)_3{\cdot}5H_2O$), and potassium bromide (KBr) was procured from Shanghai Aladdin Biochemical Science and Technology Co., Ltd. Silver nitrate ($AgNO_3$) was purchased from Shanghai Institute of Fine Chemical Materials, and ethylene glycol (EG) was sourced from Tianjin Feng Chuan Chemical Reagent Technology Co., Ltd. The synthesis of deionized water was accomplished through the MiIII-Q method. All reactants and solvents used in this study were of analytical grade and were utilized without additional purification.

Synthesis of D-BYE, A-BYE NPs

Chiral nanostructured BiOBr:10% Yb^{3+}/4% Er^{3+} (D-BYE) nanomaterials were initially synthesized using a hydrothermal method followed by calcination in air. In the first step, 0.04 mmol of Er_2O_3 and 0.1 mmol of Yb_2O_3 powders were dissolved in 40 ml of concentrated nitric acid at 180 °C. The resulting solution was then mixed with 16 ml of ethanol (EG) and 4 ml of water, followed by the addition of 1 mmol of $Bi(NO_3)_3{\cdot}5H_2O$ and 1 mmol of NaBr. After stirring for 30 minutes, 0.5 mmol of D-Sor was introduced, and the mixture was stirred for an additional 30 minutes. The solution was then transferred to a 100 ml PTFE reactor and heated at 160 °C for 12 hours. The precipitated sample was cooled to room temperature, washed several times with deionized water to remove unreacted materials and impurities, then washed with anhydrous ethanol and dried. The precursor was then calcined in a vacuum at 450 °C for 2 hours, with a ramp rate of 5 °C per minute, resulting in the formation of D-BYE powder. The yield was determined to be approximately 80%. Similarly, we employed the same procedure to synthesize the non-chiral A-BYE powders, preparing the A-BYE samples without the addition of the chiral molecule D-Sor. The yield was approximately 85%.

Synthesis of D-BYE:Ag NPs

D-BYE:*x* g Ag NPs (x = 0.03, 0.06, 0.08) were prepared using a two-step method. The first step involved a photoreductive pathway. Initially, 250 mg of D-BYE was dispersed in 20 ml of deionized water and 20 ml of EG solution, followed by vigorous stirring for 10 minutes in the dark. Silver nitrate was then added to the D-BYE suspension, and the mixture was irradiated and stirred under UV light (125 W mercury lamp) for 30 minutes, during which the white suspension gradually changed to a gray-black color. The second step employed a hydrothermal method. The mixed solution was transferred to a 100 ml PTFE reactor and heated at 160 °C for 12 hours. After cooling the precipitated sample to room temperature, it was washed several times with deionized water to remove unreacted materials and impurities, then washed with anhydrous ethanol and dried. Finally, the resulting powder was calcined at 450 °C for 2 hours at a heating rate of 5 °C min^{-1} to obtain D-BYE-*x* g Ag NPs (x = 0.03, 0.06, 0.08). The yield was approximately 95%.

Characterization

The structure properties of all the samples were examined by X-ray diffraction (Rigaku Smart Lab). Scanning electron

microscopy (SEM) images were collected using a SU8600 at an accelerating voltage of 5 kV (Hitachi, Japan). Circular dichroism spectra (CD) were recorded on a circular dichroism analyzer (JASCOJ-1500, Japan). PL spectra were measured at room temperature using a Hitachi F-7000 spectrophotometer and spectrometer (FLS980, Edinburgh, UK) with a modulated 980 nm continuous wavelength laser as the pump source. Absorption spectra were recorded using a UV-3600 (SPC, Japan). Time-resolved PL decay curves were recorded under 980 nm excitation on a FLS980 steady-state transient spectrometer (Edinburgh, UK).

Numerical simulation

The near-field electric field distribution was simulated using the FDTD method. The structural parameters for the chiral inorganic nanoparticles and the Ag particles coupled with the inorganic nanoparticle materials used in the simulations were obtained from SEM images. The near-field calculations were conducted using an incident light source with a wavelength of 980 nm, with perfectly matched layer (PML) boundaries applied along the x, y, and z axes. For the FDTD simulations, a mesh size of 1 nm was employed for the structure.

Results and discussion

Fig. 1a illustrates the XRD patterns of samples that have not undergone chiral molecular modification and that do not contain Ag particles (A-BYE) and chiral inorganic nanoparticles (D-BYE), and chiral inorganic nanoparticles coupled with varying amounts of Ag particles (D-BYE-x g Ag). All diffraction peaks for A-BYE and D-BYE correspond to the tetragonal phase of BiOBr, while those for D-BYE-x g Ag correspond to the tetragonal phases of BiOBr and $AgNO_3$. The absence of impurity peaks in the samples indicates high purity and confirms the successful coupling of inorganic nanoparticles with Ag particles. Fig. 1b shows the SEM images of A-BYE, D-BYE, and D-BYE-0.06Ag. As shown in Fig. 1b, the SEM image of the sample that has not undergone modification with a chiral molecule and that does not contain silver particles (A-BYE) reveals microspheres formed by the stacking of numerous small nanosheets. Here, we chose D-Sor as a symmetry-breaking agent and structure-directing agent, the SEM image of chiral inorganic nanoparticles (D-BYE) shows a significant transformation, with the structure changing to petal-like microspheres created by the rotational stacking of small nanosheets. When Ag particles are added (D-BYE-0.06Ag), the

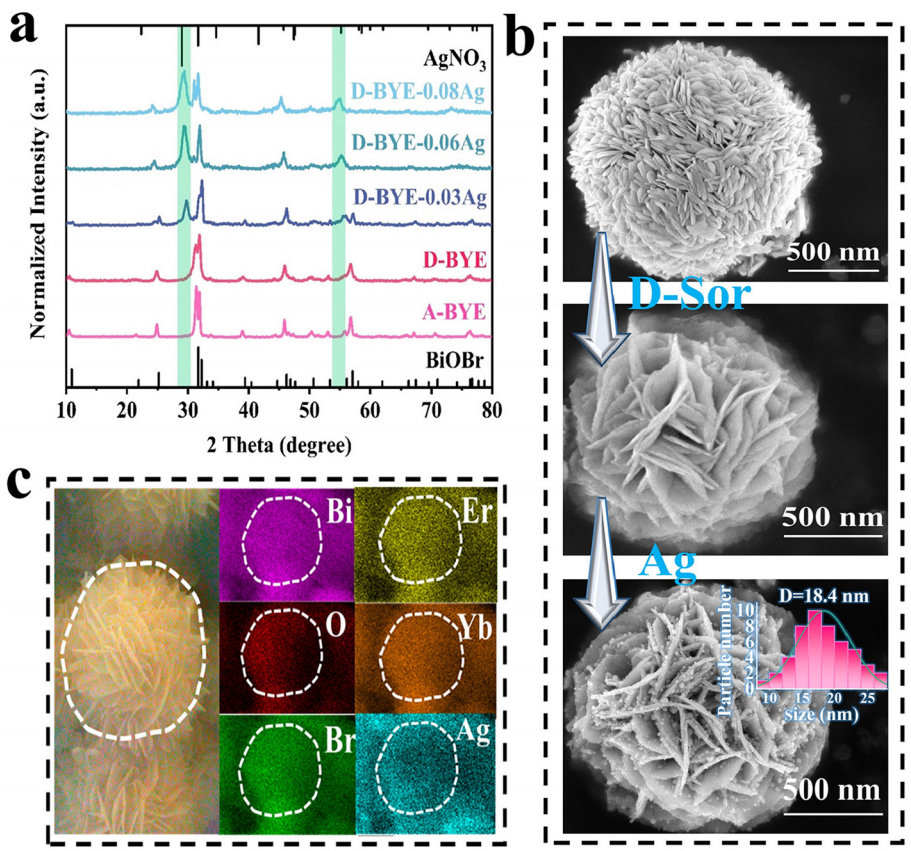

Fig. 1 (a) XRD patterns of D-BYE-x g Ag (x = 0.03, 0.06, 0.08) and D-BYE, A-BYE. The black diffraction curve at the bottom represents the standard pattern of BiOBr, and the black diffraction curve at the top represents the standard pattern of $AgNO_3$. (b) SEM image of A-BYE, D-BYE, D-BYE-0.06Ag. (c) SEM image and the corresponding EDS mapping of Bi, O, Br, Er, Yb, Ag elements in the D-BYE-0.06Ag sample.

SEM image clearly shows many Ag particles coupled to the petal-like microspheres. In the upper right of the SEM image of D-BYE-0.06Ag, the average particle size of the silver particles distributed on the petal sphere is indicated, with a value of approximately 18.4 nm. Elemental mapping further confirmed the presence of Bi, O, Br, Er, Yb, and Ag in the D-BYE-0.06Ag sample (Fig. 1c). The above characterization confirms the successful preparation of samples with Ag particles coupled to chiral inorganic nanostructures.

We further investigated the UCL properties of samples composed of chiral inorganic nanoparticles coupled with Ag particles. The UCL spectra of A-BYE, D-BYE, and D-BYE-*x* g Ag (x = 0.03, 0.06, 0.08) under 980 nm laser excitation are presented in Fig. 2a. These spectra clearly reveal green emission at 550 nm and red emission at 674 nm, corresponding to the transitions of Er^{3+} ions: $^4S_{3/2} \rightarrow {}^4I_{15/2}$ and $^4F_{9/2} \rightarrow {}^4I_{15/2}$ (as illustrated in Fig. S2†). Notably, the UCL is significantly enhanced by the coupling between Ag particles and the chiral inorganic nanoparticles. The specific enhancement factors are shown in Fig. 2b. Compared to A-BYE, the UCL intensity of D-BYE-0.06Ag showed a remarkable increase, with a maximum enhancement of 75 times in green light and 87 times in red light. When excited by 980 nm light, silver particles generate a LSPR, resulting in the formation of a highly concentrated electromagnetic field at the particle surface. This strong electromagnetic field interacts with the chiral material, dramatically increasing the strength of the chiral field and thereby significantly increasing the luminescence intensity.[29–34] To characterize the UP-CPL performance of D-BYE-0.06Ag, a quarter-wave plate (QWP) and a polarizer (PL) were placed in front of the spectrometer to generate different polarization states under 980 nm laser excitation. By setting the angle $\alpha = -45°$ between the polarizer and the optical axis of the QWP, left circularly polarized light (LCP) was produced. Conversely, setting the angle $\alpha = 45°$ resulted in the production of right circularly polarized light (RCP). For chiral inorganic nanomaterials coupled with Ag particles, the surface plasmon resonance may lead to a more pronounced local field enhancement for right circularly polarized light. This effect can further amplify the luminescence intensity of the RCP, resulting in a greater RCP intensity compared to LCP, as illustrated in Fig. 2d.[35] The results of our control experiments, as shown in Fig. S1,† demonstrate that there is virtually no difference between the UCL intensities of LCP and RCP for A-BYE. As shown in Fig. 2e, a change is observed in the differential CPL spectra of D-BYE-0.06Ag, while no change is observed in A-BYE (defined as ΔCPL = RCP − LCP). As shown in Fig. 2c and f, the PL decay lifetimes at 550 nm and 674 nm for the D-BYE-0.06 Ag sample are significantly longer than those for the A-BYE sample. The enhancement of the local field reduces non-radiative energy transfer. Specifically, the increased electromagnetic field can decrease the amount of energy dissi-

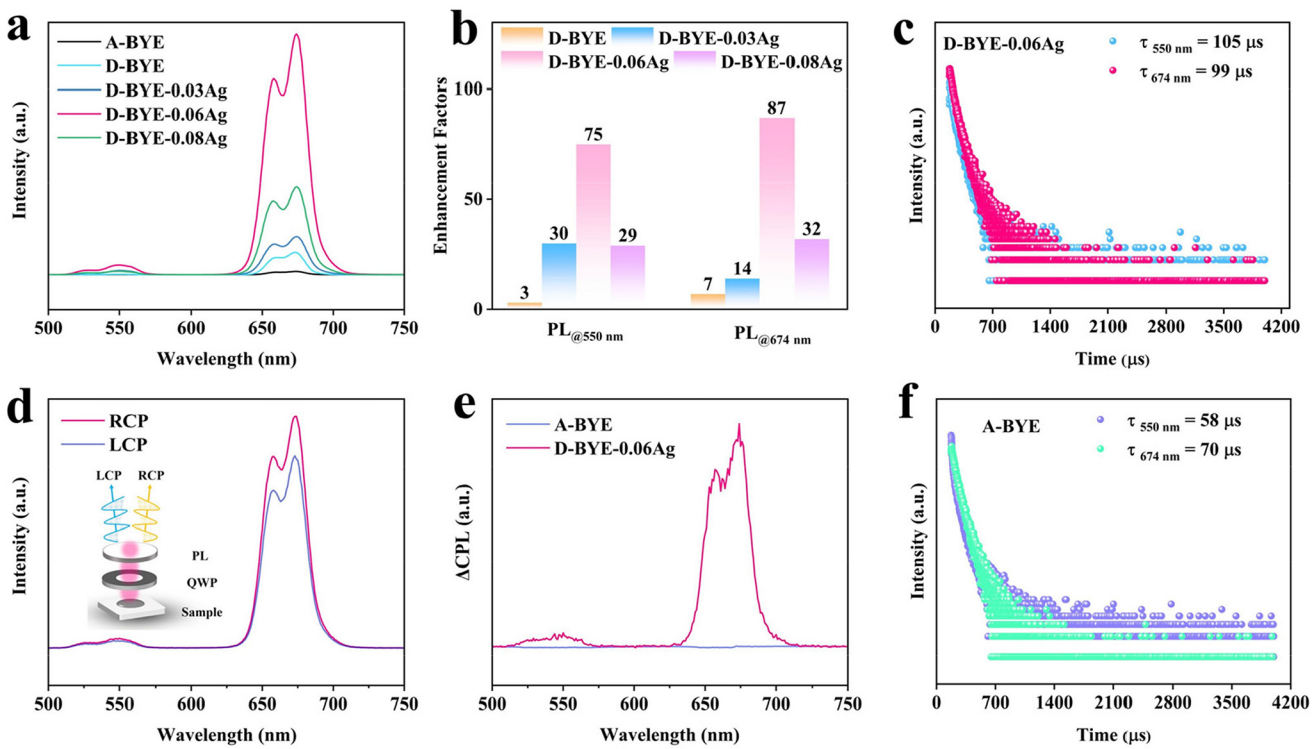

Fig. 2 (a) PL spectra of D-BYE-*x* g Ag (x = 0.03, 0.06, 0.08) and D-BYE, A-BYE samples under 980 nm laser excitation. (b) Enhancement factor of D-BYE and D-BYE-0.06Ag relative to A-BYE at wavelengths of 550 nm and 674 nm. (c) PL decay curves of D-BYE-0.06Ag under 980 nm excitation at 550 nm and 674 nm. (d) LCP and RCP UCL from the D-BYE-0.06Ag. The schematic illustrates the generation of the LCP and RCP. (e) Differentiated CPL spectra of D-BYE-0.06Ag and A-BYE. (f) PL decay curves of A-BYE under 980 nm excitation at 550 nm and 675 nm.

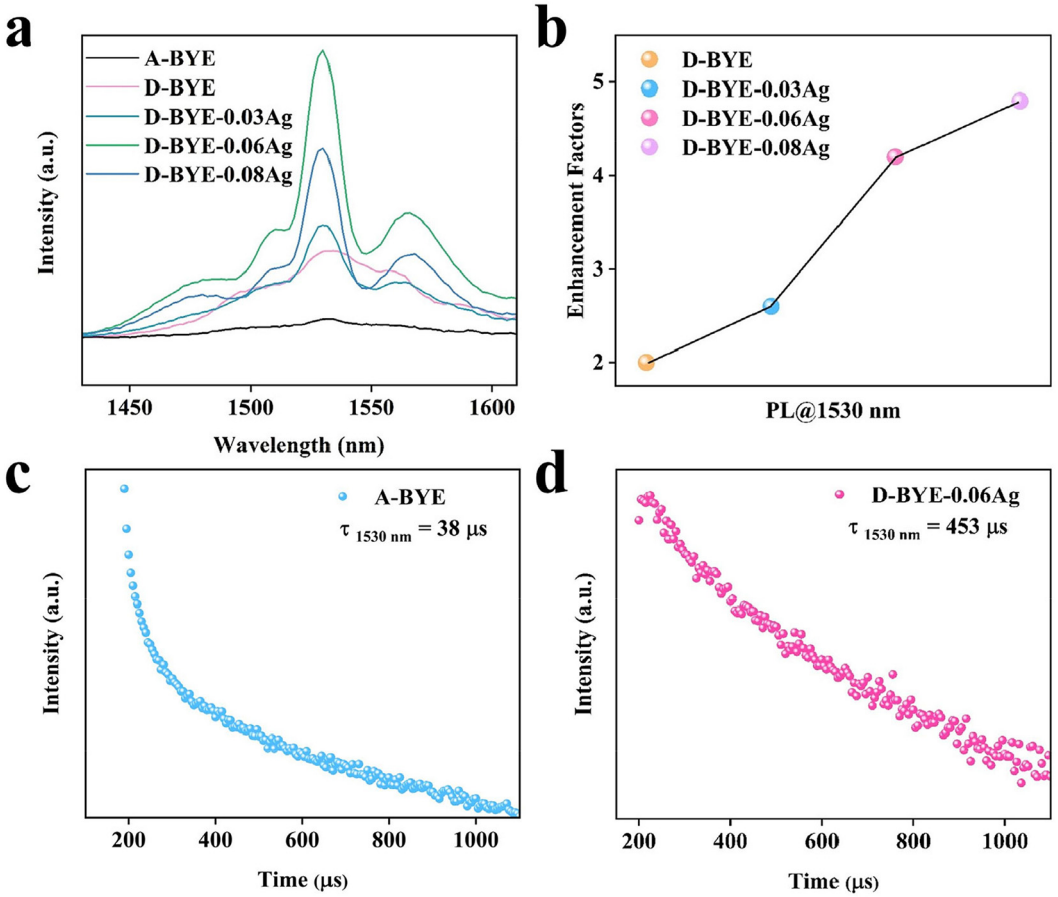

Fig. 3 (a) PL spectra of D-BYE-*x* g Ag (*x* = 0.03, 0.06, 0.08) and D-BYE, A-BYE samples under 980 nm laser excitation. (b) Enhancement factor of D-BYE and D-BYE-0.06Ag relative to A-BYE at wavelengths of 1530 nm. (c) The PL decay curves of A-BYE under 980 nm excitation at 1530 nm. (d) The PL decay curves of D-BYE-0.06Ag under 980 nm excitation at 1530 nm.

pated through non-radiative processes, thereby extending the fluorescence lifetime.

SPR is an effective method for enhancing upconversion luminescence intensity and broadening its applications. Consequently, we examine its role in the near-infrared region. Fig. 3a illustrates the PL spectra of D-BYE-*x* g Ag (*x* = 0.03, 0.06, 0.08) and D-BYE, A-BYE samples under 980 nm laser excitation. Compared to the D-BYE and A-BYE samples, the emission intensity of D-BYE-*x* g Ag increases progressively with the $AgNO_3$ content. However, when the $AgNO_3$ content reaches 0.08 g, a slight decrease in emission intensity is observed, although it remains higher than that of the D-BYE and A-BYE samples. The maximum enhancement of the emission intensity at 1530 nm for D-BYE-0.06Ag, calculated as a ratio of integral intensities, is five times greater than that of A-BYE, as shown in Fig. 3b. The emission peak at 1530 nm corresponds to the $^4I_{13/2} \rightarrow {}^4I_{15/2}$ transition of the Er^{3+} ion (as illustrated in Fig. S2†). As shown in Fig. S3 and S4,† the coupling of silver nanoparticles with chiral inorganic nanostructures results in strong and narrow emission in the NIR region, in contrast to the chiral inorganic nanostructured samples. The significant enhancement of fluorescence can be attributed to several factors: the reduced optical loss of Ag particles in the NIR region, the realization of a stronger resonance through Mie scattering, and the Mie enhancement effect in the NIR range. In the NIR region, the optical loss of Ag particles typically decreases. This behavior can be understood by examining the complex dielectric constant and plasma frequency of Ag. The complex permittivity of Ag is often expressed as:

$$\varepsilon(\lambda) = \varepsilon_1(\lambda) + i\varepsilon_2(\lambda) \quad (1)$$

where, $\varepsilon_1(\lambda)$ represents the real part, which describes the electric field response of Ag. $\varepsilon_2(\lambda)$ represents the imaginary part, which is directly related to light absorption and reflects the material's loss characteristics. In the visible region, particularly near the blue-violet part of the spectrum, Ag exhibits higher optical losses. This is because, at these wavelengths, the free electrons in silver respond strongly to electromagnetic waves, leading to significant absorption. As the wavelength increases towards the NIR region, the imaginary part $\varepsilon_2(\lambda)$ the complex permittivity generally decreases. This reduction indicates a decrease in absorption loss.

In summary, the enhancement of the Mie scattering resonance effect is attributed to the reduction in light loss of Ag particles in the NIR region.[36–39] This increased resonance effect results in the emission spectra peaks becoming sharper and narrower. Based on previous reports, the fluorescence lifetime of chiral inorganic nanoparticles is typically reduced. However, as shown in Fig. 3c and d, when Ag particles are coupled with chiral inorganic nanoparticles, the fluorescence lifetime is extended compared to A-BYE. This extension can be attributed to the surface plasmon resonance effect of the Ag nanoparticles, which concentrates and enhances the local electromagnetic field. This effect increases the material's radiative transition efficiency while reducing energy dissipation through non-radiative transitions.

To elucidate the potential effects of plasma and the influence of energy band structure on optical properties. Consequently, the UV-vis absorption spectra were employed to evaluate the optical absorption characteristics of the prepared A-BYE, D-BYE, and D-BYE-0.06Ag samples. As illustrated in Fig. 4a, the D-BYE-0.06Ag sample shows a slight redshift in comparison to A-BYE. This shift suggests a narrowing of the band gap in the sample, which leads to improved visible light absorption, due to the presence of Ag particles. As illustrated in Fig. 4b and d, the bandgap of D-BYE-0.06Ag is markedly smaller than that of A-BYE. The SPR effect of Ag metal nanoparticles lead to a significant redshift in the absorption peaks and a reduction in the bandgap. Materials with a chiral structure exhibit selective interaction with CPL, which gives rise to the phenomenon of optical activity. This phenomenon can be characterized by CD spectroscopy. As shown in Fig. 4c, the CD spectrum of the D-BYE sample exhibits a strong positive peak in the range of 370–410 nm, indicating a disruption in symmetry. In contrast, the D-BYE-0.06Ag sample also shows a strong positive peak, but within the range of 385–450 nm, accompanied by a pronounced redshift. This redshift is attributed to the coupling between Ag nanoparticles and the chiral nanomaterials, due to the LSPR effect of the silver nanoparticles.[40,41] Meanwhile, the A-BYE sample exhibited almost no signal in the 370–450 nm range, providing further evidence that the system of Ag particles coupled with chiral inorganic nanomaterials, exhibits chiral characteristics.

To gain deeper insights into the luminescence enhancement mechanism in the system of Ag particles coupled with chiral inorganic nanomaterials, we investigated the electric field enhancement effect for the D-BYE and D-BYE-0.06Ag samples, as shown in Fig. 5. The dielectric constant (ε = 6.38) of the D-BYE sample was calculated using first-principles methods, as shown in Fig. S5.† Because the helix line is a

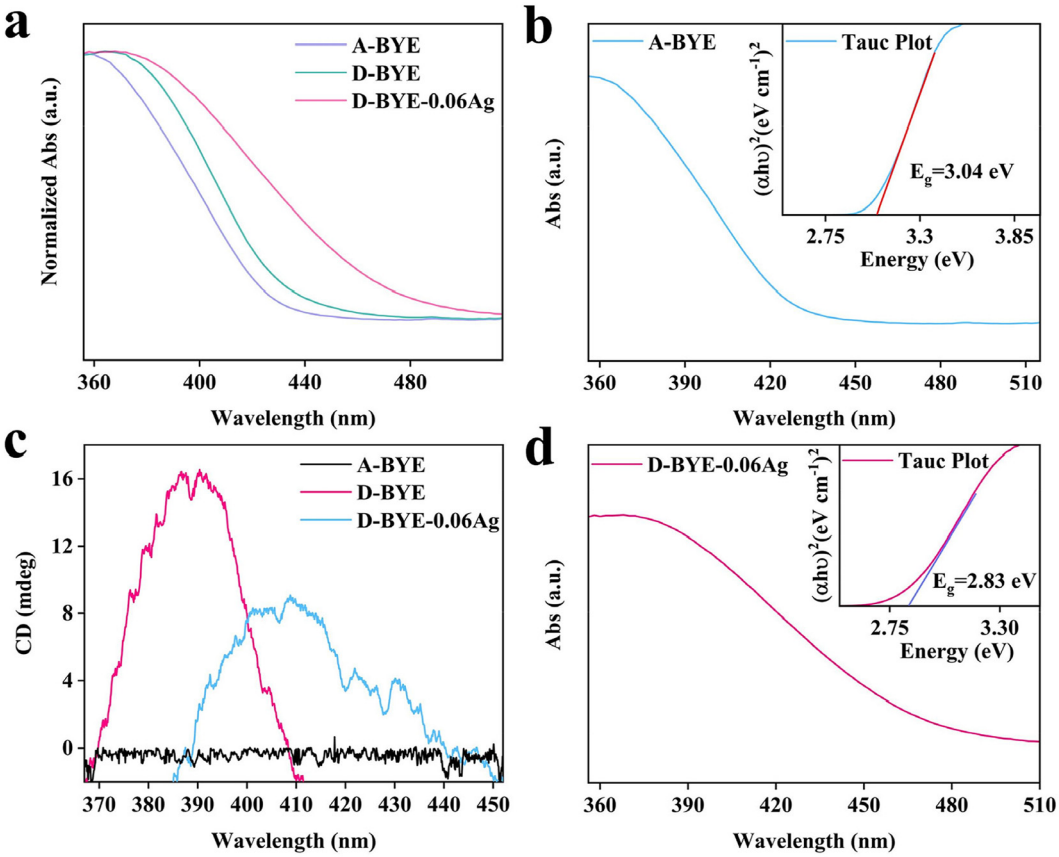

Fig. 4 (a) The UV-Vis absorption spectra of D-BYE-0.06 Ag and D-BYE, A-BYE samples. (b) Absorption spectra and Tauc plots of A-BYE. (c) CD spectra of A-BYE and D-BYE, D-BYE-0.06Ag. (d) Absorption spectra and Tauc plots of D-BYE-0.06Ag.

typical helical symmetry structure, it is inherently chiral. Therefore, we choose the helix line as the chiral structure model. The primary structural parameters of this model include the pitch, the diameter of the helix, the helix radius, and the radius of the coupled silver particles, all of which are derived from SEM measurements of the samples. A PML boundary was employed along the x, y, and z axes, using an incident light source with a wavelength of 980 nm. We then employed FDTD simulation software to model the D-BYE (Fig. S6†) and D-BYE-0.06Ag samples (Fig. S7†) to analyze their electric field enhancement effects. The results indicate that both the chiral helical structures D-BYE and D-BYE-0.06Ag generate localized fields under 980 nm laser excitation. However, the system incorporating Ag particles coupled with chiral inorganic nanomaterials produces stronger electromagnetic fields compared to the chiral helical structures alone, as shown in Fig. 5 and Fig. S8, 9.† This enhancement can be attributed to the coupling between the Ag particles and the chiral nanomaterials. This coupling amplifies the localized strength of the electromagnetic field. Specifically, silver particles excited by 980 nm light produce LSPR, generating a very strong localized electromagnetic field at their surface. When these silver particles are coupled with chiral nanomaterials, the locally enhanced electromagnetic field interacts with the chiral materials, enhancing the strength of the chiral field. Therefore, Ag particles coupled with chiral inorganic nanomaterials, in the presence of a strong electromagnetic field, result in an accelerated radiative transition rate and a reduced probability of non-radiative transitions, leading to enhanced luminescence.

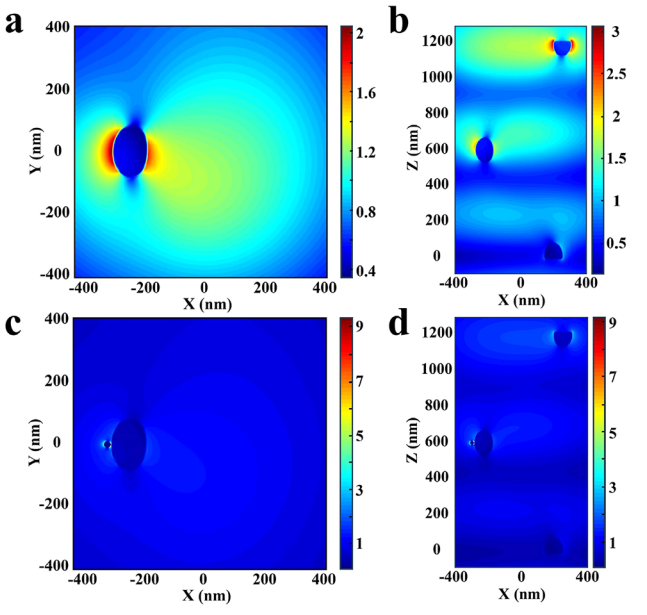

Fig. 5 (a and b) Electromagnetic field distribution in the X–$Y(Z)$ plane obtained from an FDTD simulation of the D-BYE. (c and d) Electromagnetic field distribution in the X–$Y(Z)$ plane obtained from an FDTD simulation of the D-BYE-0.06Ag.

Conclusion

In summary, we have experimentally investigated the optical properties of materials formed by the coupling of Ag particles with chiral inorganic nanoparticles. Enhanced and upconverted polarized light of luminescence in the visible to near-infrared region can be achieved through the coupling of Ag particles with chiral inorganic nanoparticles. The near-field electric field and its optical chirality have been investigated using the FDTD method to elucidate their mechanisms. Under the excitation of 980 nm light, silver particles exhibit LSPR, generating a highly concentrated electromagnetic field on their surfaces. This enhanced electromagnetic field interacts with the chiral material, thereby further amplifying the strength of the chiral field. Significant luminescence enhancement in the visible to near-infrared region is observed in materials with Ag particle coupling, with maximum enhancement coefficients of 75 and 87 in the 550 nm and 674 nm bands, respectively, and a coefficient of 5 in the near-infrared region at the 1530 nm band. Combining plasmonic nanostructures can effectively modulate both emission intensity and polarization, offering a promising approach to enhancing luminescence efficiency.

Data availability

All data generated or analysed during this study are included in this published article.

Conflicts of interest

There are no conflicts to declare.

Acknowledgements

This work was supported by the National Natural Science Foundation of China-Yunnan Joint Fund (U1902222, U2241236), the National Natural Science Foundation of China (12204206, 11774138, 12064021, 51862020), the Yunnan Fundamental Research Projects (No. 202201AT070174, 202301AT070149, 202001AT070037, 202101AT070104, 202101AT070097).

References

1 K. Saito and T. Tatsuma, Chiral Plasmonic Nanostructures Fabricated by Circularly Polarized Light, *Nano Lett.*, 2018, **18**(5), 3209–3212.
2 D. Han, C. Li, C. Jiang, X. Jin, X. Wang, R. Chen, J. Cheng and P. Duan, Endowing inorganic nanomaterials with circularly polarized luminescence, *Aggregate*, 2021, **3**(1), e148.
3 K. Ding, J. Ai, Q. Deng, B. Huang, C. Zhou, T. Duan, Y. Duan, L. Han, J. Jiang and S. Che, Chiral Mesostructured

BiOBr Films with Circularly Polarized Colour Response, *Angew. Chem., Int. Ed.*, 2021, **60**(35), 19024–19029.
4 J. George, S. Kar, E. S. Anupriya, S. M. Somasundaran, A. D. Das, C. Sissa, A. Painelli and K. G. Thomas, Chiral Plasmons: Au Nanoparticle Assemblies on Thermoresponsive Organic Templates, *ACS Nano*, 2019, **13**(4), 4392–4401.
5 C. L. Chen and N. L. Rosi, Peptide–Based Methods for the Preparation of Nanostructured Inorganic Materials, *Angew. Chem., Int. Ed.*, 2010, **49**(11), 1924–1942.
6 Y. Guan, Z. Wang, B. Ai, C. Chen, W. Zhang, Y. Wang and G. Zhang, Chiral Plasmonic Metamaterials with Tunable Chirality, *ACS Appl. Mater. Interfaces*, 2020, **12**(44), 50192–50202.
7 H. Gao, C. Zhan, T. Zhao and J. Zheng, Chirality transfer induced circularly polarized luminescence of achiral dye molecules by plasmonic nanohelicoid, *Nano Res.*, 2024, **17**(9), 8408–8414.
8 W. Du, X. Wen, D. Gérard, C.-W. Qiu and Q. Xiong, Chiral plasmonics and enhanced chiral light-matter interactions, *Sci. China:Phys., Mech. Astron.*, 2019, **63**(4), 244201.
9 H. He, M. Cen, J. Wang, Y. Xu, J. Liu, W. Cai, D. Kong, K. Li, D. Luo, T. Cao and Y. J. Liu, Plasmonic Chiral Metasurface-Induced Upconverted Circularly Polarized Luminescence from Achiral Upconversion Nanoparticles, *ACS Appl. Mater. Interfaces*, 2022, **14**(48), 53981–53989.
10 T. Zhao, D. Meng, Z. Hu, W. Sun, Y. Ji, J. Han, X. Jin, X. Wu and P. Duan, Enhanced chiroptic properties of nanocomposites of achiral plasmonic nanoparticles decorated with chiral dye-loaded micelles, *Nat. Commun.*, 2023, **14**(1), 81.
11 J. Chen, X. Gao, Q. Zheng, J. Liu, D. Meng, H. Li, R. Cai, H. Fan, Y. Ji and X. Wu, Bottom-Up Synthesis of Helical Plasmonic Nanorods and Their Application in Generating Circularly Polarized Luminescence, *ACS Nano*, 2021, **15**(9), 15114–15122.
12 J. H. Han, D. Kim, J. Kim, G. Kim, P. Fischer and H. H. Jeong, Plasmonic Nanostructure Engineering with Shadow Growth, *Adv. Mater.*, 2022, **35**(34), 2107919.
13 J. Guo, G. Song, Y. Huang, K. Liang, F. Wu, R. Jiao and L. Yu, Optical Chirality in a Strong Coupling System with Surface Plasmons Polaritons and Chiral Emitters, *ACS Photonics*, 2021, **8**(3), 901–906.
14 Z. Huang and J. Liu, Chiroptically Active Metallic Nanohelices with Helical Anisotropy, *Small*, 2017, **13**(43), 1701883.
15 U. Kilic, M. Hilfiker, A. Ruder, R. Feder, E. Schubert, M. Schubert and C. Argyropoulos, Broadband Enhanced Chirality with Tunable Response in Hybrid Plasmonic Helical Metamaterials, *Adv. Funct. Mater.*, 2021, **31**(20), 2010329.
16 A. Guerrero-Martínez, J. L. Alonso-Gómez, B. Auguié, M. M. Cid and L. M. Liz-Marzán, From individual to collective chirality in metal nanoparticles, *Nano Today*, 2011, **6**(4), 381–400.
17 M. Hentschel, M. Schäferling, X. Duan, H. Giessen and N. Liu, Chiral plasmonics, *Sci. Adv.*, 2017, **3**(5), e1602735.
18 J. Wang, X. Wu, W. Ma and C. Xu, Chiral AuCuAu Heterogeneous Nanorods with Tailored Optical Activity, *Adv. Funct. Mater.*, 2020, **30**(17), 2000670.
19 L. Nguyen, M. Dass, M. F. Ober, L. V. Besteiro, Z. M. Wang, B. Nickel, A. O. Govorov, T. Liedl and A. Heuer-Jungemann, Chiral Assembly of Gold–Silver Core–Shell Plasmonic Nanorods on DNA Origami with Strong Optical Activity, *ACS Nano*, 2020, **14**(6), 7454–7461.
20 L. Yang, P. Nandi, Y. Ma, J. Liu, U. Mirsaidov and Z. Huang, Binary Chiral Nanoparticles Exhibit Amplified Optical Activity and Enhanced Refractive Index Sensitivity, *Small*, 2020, **16**(6), 1906048.
21 M. Saboktakin, X. Ye, U. K. Chettiar, N. Engheta, C. B. Murray and C. R. Kagan, Plasmonic Enhancement of Nanophosphor Upconversion Luminescence in Au Nanohole Arrays, *ACS Nano*, 2013, **7**(8), 7186–7192.
22 L. Wang, S. Guo, D. Liu, J. He, J. Zhou, K. Zhang, Y. Wei, Y. Pan, C. Gao, Z. Yuan, D. Lei, X. Xie and L. Huang, Plasmon–Enhanced Blue Upconversion Luminescence by Indium Nanocrystals, *Adv. Funct. Mater.*, 2019, **29**(29), 1901242.
23 B. Kalinic, T. Cesca, C. Scian, N. Michieli, I. G. Balasa, E. Trave and G. Mattei, Emission Efficiency Enhancement of Er^{3+} Ions in Silica by Near–Field Coupling With Plasmonic and Pre–Plasmonic Nanostructures, *Phys. Status Solidi A*, 2017, **215**(3), 1700437.
24 Y. Wu, J. Xu, E. T. Poh, L. Liang, H. Liu, J. K. W. Yang, C.-W. Qiu, R. A. L. Vallée and X. Liu, Upconversion superburst with sub-2 μs lifetime, *Nat. Nanotechnol.*, 2019, **14**(12), 1110–1115.
25 H. Chen, Z. Jiang, H. Hu, B. Kang, B. Zhang, X. Mi, L. Guo, C. Zhang, J. Li, J. Lu, L. Yan, Z. Fu, Z. Zhang, H. Zheng and H. Xu, Sub-50-ns ultrafast upconversion luminescence of a rare-earth-doped nanoparticle, *Nat. Photonics*, 2022, **16**(9), 651–657.
26 X. Chen, W. Xu, L. Zhang, X. Bai, S. Cui, D. Zhou, Z. Yin, H. Song and D. H. Kim, Large Upconversion Enhancement in the "Islands" Au–Ag Alloy/$NaYF_4$: Yb^{3+}, Tm^{3+}/Er^{3+} Composite Films, and Fingerprint Identification, *Adv. Funct. Mater.*, 2015, **25**(34), 5462–5471.
27 D.-R. Jung, J. Kim, C. Nahm, S. Nam, J. I. Kim and B. Park, Surface-plasmon-enhanced photoluminescence of CdS nanoparticles with Au/SiO_2 nanocomposites, *Mater. Res. Bull.*, 2012, **47**(2), 453–457.
28 P. Lu, C. Cai, B. Zhang, B. Liu, H. Wu, G. Bi and J. Si, Plasmonically-enhanced mid-infrared photoluminescence in a metal/narrow-gap semiconductor structure, *EPL*, 2016, **114**(3), 37005.
29 L. Wang, M. Hasanzadeh Kafshgari and M. Meunier, Optical Properties and Applications of Plasmonic–Metal Nanoparticles, *Adv. Funct. Mater.*, 2020, **30**(51), 200540.
30 W. Park, D. Lu and S. Ahn, Plasmon enhancement of luminescence upconversion, *Chem. Soc. Rev.*, 2015, **44**(10), 2940–2962.
31 H. Zong, X. Mu and M. Sun, Physical principle and advances in plasmon-enhanced upconversion luminescence, *Appl. Mater. Today*, 2019, **15**, 43–57.

32 Z. Wang, C. Wang, Q. Han, G. Wang, M. Zhang, J. Zhang, W. Gao and H. Zheng, Metal-enhanced upconversion luminescence of $NaYF_4$:Yb/Er with Ag nanoparticles, *Mater. Res. Bull.*, 2017, **88**, 182–187.
33 L. Hu, Z. Sun, Y. Nie, Y. Huang and Y. Fang, Plasmonic and Photonic Enhancement of Chiral Near–Fields, *Laser Photonics Rev.*, 2022, **16**(11), 2200035.
34 Z. Wang, Y. Wang, G. Adamo, J. Teng and H. Sun, Induced Optical Chirality and Circularly Polarized Emission from Achiral CdSe/ZnS Quantum Dots via Resonantly Coupling with Plasmonic Chiral Metasurfaces, *Laser Photonics Rev.*, 2019, **13**(3), 1800276.
35 R. Ma, H. Zhang, Y. Lang, Y. Li, Z. Song, D. Zhou, Q. Wang, Z. Long, Y. Yang, Y. Wen, Y. Gao, J. Han and J. Qiu, Boosted luminescence of chiral nanophosphors with circularly polarized luminescence, *Ceram. Int.*, 2024, **50**(20), 39823–39829.
36 Y. Liang, D. P. Tsai and Y. Kivshar, From Local to Nonlocal High-Q Plasmonic Metasurfaces, *Phys. Rev. Lett.*, 2024, **133**(5), 053801.
37 Y. Kivshar, The Rise of Mie-tronics, *Nano Lett.*, 2022, **22**(9), 3513–3515.
38 X. Shan, G. Tang, X. Chen, S. Peng, W. Liu, Q. Qian, D. Chen and Z. Yang, Silver nanoparticles enhanced near-infrared luminescence of Er^{3+}/Yb^{3+} co-doped multicomponent phosphate glasses, *J. Rare Earths*, 2016, **34**(9), 868–875.
39 Z. Li, G. Geng, J. Cheng, W. Liu, S. Yu, B. Xie, H. Cheng, J. Li, W. Zhou, J. Tian and S. Chen, Flexible Confinement and Manipulation of Mie Resonances via Nano Rectangular Hollow Metasurfaces, *Adv. Opt. Mater.*, 2022, **10**(13), 2200185.
40 P. M. Nithya and L. G. Devi, Effect of surface Ag metallization on the photocatalytic properties of $BaTiO_3$: Surface plasmon effect and variation in the Schottky barrier height, *Surf. Interfaces*, 2019, **15**, 205–215.
41 A. Raturi, P. Mittal and S. Choudhary, Tuning the electronic and optical properties of $SrTiO_3$ for optoelectronic and photocatalytic applications by plasmonic-metal doping: a DFT-computation, *Opt. Quantum Electron.*, 2022, **54**(10), 634.